Low-cost hybrid design of masonry structures for developing countries: Shaking table tests

Journal Article

Author(s):
Tsiavos, Anastasios; Sextos, Anastasios; Stavridis, Andreas; Dietz, Matt; Dihoru, Luiza; Di Michele, Francesco; Alexander, Nicholas A.
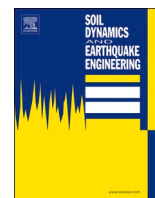
Low-cost hybrid design of masonry structures for developing countries: Shaking table tests

Anastasios Tsiavos [a,*], Anastasios Sextos [b], Andreas Stavridis [c], Matt Dietz [d], Luiza Dihoru [d], Francesco Di Michele [e], Nicholas A. Alexander [f]

[a] Lecturer, Department of Civil, Environmental and Geomatic Engineering, ETH Zurich, Switzerland
[b] Professor of Earthquake Engineering and Head of Earthquake and Geotechnical Engineering Research Group, Department of Civil Engineering, University of Bristol, UK
[c] Department of Civil, Structural and Environmental Engineering, University at Buffalo, United States
[d] Research Fellow, Department of Civil Engineering, University of Bristol, UK
[e] PhD Student, Department of Civil Engineering, University of Bristol, UK
[f] Associate Professor in Structural Dynamics, Department of Civil Engineering, University of Bristol, UK

ABSTRACT

This study presents a large-scale shaking table investigation aimed at the development of a dual, low-cost hybrid design approach for the reduction of seismic damage in developing countries. The introduction of a novel seismic isolation strategy, defined as 'PVC sand-wich' seismic isolation lies in the core of the proposed hybrid approach. The latter relates to conventional, 'good practice' design (including steel wire mesh wall retrofit and connecting ties) that permits strength-based resistance to lateral loads for intensity up to the design earthquake combined with a sliding 'fuse' mechanism that is triggered once the above threshold is exceeded. A three times scaled-down seismically isolated masonry model of a prototype structure located in Nepal is designed, constructed according to the proposed design approach and tested to earthquake ground motion excitations on a 3 m × 3 m shaking table. The efficiency of the proposed design approach is assessed through the experimental investigation of the seismically isolated structure, while the seismic response of the corresponding unretrofitted masonry structure is simulated numerically. The results demonstrate that the PVC sand-wich isolation mechanism can be a promising alternative to more expensive damage mitigating solutions.

1. Introduction

The documented damage and casualties due to the destructive 2015 Gorkha earthquake [1] have highlighted the necessity for the design of locally resourced, low-cost, yet efficient, engineering measures to mitigate seismic risk [2] in developing countries [3].

The seismic isolation of structures using frictional [4] or elastomeric devices [5] has been well established in the last decades as an efficient means to reduce seismic damage in developed countries [6–8] and applied in a wide variety of structural systems [9–13] due to its ability to protect the structure above a predetermined critical acceleration threshold. Nonetheless, the financial resources required for the implementation of existing seismic isolation techniques are prohibitive in developing countries.

Thus, a breadth of different low-cost seismic isolation systems based on soil and recycled rubber have been proposed; Gazetas [14] and

Anastasopoulos et al. [15] have introduced the concept of plastic hinging within the foundation-soil system to promote a rocking form of isolation, which was extended to liquefiable soils by Karatzia et al. [16] and to limestone sand by Banovic et al. [17]. Recognizing the environmental advantages due to the use of rubber recycled from car tyres, Tsang et al. [18,19] and Mitoulis et al. [20] have explored the use of soil-rubber mixtures for the design of low-cost seismic isolation. Tsiavos et al. [21] have investigated experimentally the use of a sand-rubber mixture for the development of a low-cost sliding seismic isolation system, characterized by a friction coefficient $\mu = 0.4$.

Evidently, a significantly lower value of friction coefficient $\mu = 0.2$ has been observed during the experimental investigation of the rolling-sliding motion of structures. The mechanisms of rolling friction have been examined in detail by Amontons [22], Tabor [23] and Eldredge and Tabor [24]. O'Rourke et al. [25] have demonstrated experimentally that the presence of a rolling mechanism initiated between sand

particles and a relatively soft polymer surface, such as PVC (PolyVinyl Chloride), decreases the interference and interlocking between the sand particles. Fang et al. [26], Dietz [27] and Lings and Dietz [28] have presented the criteria according to which sand particles exhibit sliding or rolling movement when they are sandwiched between two interfaces. The experimentally observed rolling movement was found to be initiated at a lower average friction coefficient, albeit associated with higher friction fluctuations over time, compared to the sliding movement. A more recent experimental investigation of the strength of polypropylene against granular materials by de Leeuw et al. [29] aimed at the design of offshore engineering projects has corroborated this favourable frictional behavior between sand particles and polymer materials. Nevertheless, this attractive sand-polymer behavior has not been utilized in the past towards the design of a novel seismic isolation system.

The design of such a novel seismic isolation system necessitates the determination of several design parameters, such as the frictional strength of the sliding interface. However, the friction coefficient characterizing the strength of a wide variety of existing seismic isolation systems manifests a significant design variation range as shown by Furinghetti et al. [30]. Moreover, the quality control in the field is linked to several uncertainties related to the nature of the selected materials and the insufficiency of advanced technical equipment in developing countries, which does not allow for a project-specific testing of the static and dynamic behavior of the seismic isolation system. Within this context, a potential underestimation of the frictional strength of a sliding seismic isolation system could significantly inhibit the activation of sliding and the robustness of the proposed seismic isolation. The reduced efficiency and activation of the isolation system could in turn damage the seismically isolated structure. In the case of masonry structures, which constitute an important percentage of new and existing structures in developing countries [1,2], this damage is commonly related to out-of-plane-failure of unreinforced masonry walls. ElGawady et al. [31], Shermi and Dubey [32] and Kouris and Triantafillou [33] have proposed the use of welded wire mesh for the seismic retrofitting of these structures against out-of-plane failure.

The aforementioned uncertainties related to the inaccurate estimation and control of the properties of a low-cost seismic isolation system for developing countries and the potential impact of this inaccurate estimation on the seismic damage of structures necessitate the integration of several seismic protection mechanisms in a wider hybrid design approach.

Along these lines, this study aims at synthesizing the benefits of three independent seismic protection mechanisms in a hybrid design approach for developing countries: The first mechanism comprises an innovative seismic isolation system, which is defined as PVC 'sand-wich' (PVC-s) seismic isolation and is based on the presented attractive initiation of sliding-rolling behavior of sand particles between two PVC surfaces. This mechanism is designed to protect the structure from earthquake ground motion intensities exceeding the friction coefficient of the sliding interface. The second and third component of the approach include the attachment of a steel wire mesh and steel ties on the surface of the outer walls of the structure for their seismic protection against in-plane and out-of-plane failure. These two mechanisms facilitate the seismic protection of the structure for earthquake ground motion intensities smaller than the friction coefficient of the sliding interface and allow for a secondary seismic protection system in case of no activation of the seismic isolation. The combined action of these mechanisms aims to respond to the challenge of a robust and low-cost design strategy for seismic damage mitigation in developing countries.

The efficiency and the beneficial role of the activation of the PVC-s seismic isolation for a large-scale steel structure subjected to an ensemble of earthquake ground motion excitations of varying frequency characteristics has been experimentally demonstrated by Tsiavos et al. [34]. However, the combined action of the three aforementioned mechanisms for the protection of a masonry structure from seismic damage has not been experimentally investigated in the past. The

efficiency of the combination of the three mechanisms presented above towards the protection of masonry structures from seismic damage is evaluated in this study through the conduction of large-scale shaking table tests at University of Bristol. A seismically isolated structure retrofitted using all the seismic protection mechanisms of the hybrid design approach is subjected to four different earthquake ground motion intensities. A numerical simulation of the seismic response of an unretrofitted masonry structure in Nepal with the same geometry is presented to determine the amount of seismic damage that would have been prevented in the unretrofitted structure by the use of the seismic protection mechanisms proposed in this study. This comparison aims to highlight the efficiency of the low-cost hybrid design approach presented in this study towards the reduction of seismic damage in developing countries.

2. Low-cost hybrid design (LC-HD): concept and application to a prototype structure

The prototype structure, presented in Fig. 1, is a typical one-storey masonry school building located in Nepal. The horizontal dimensions of this structure are 4 m × 6 m, while the height is 3 m. The thickness of the masonry walls is 30 cm.

The prototype structure is seismically retrofitted using the novel design approach proposed in this study, defined as Low-Cost Hybrid Design (LC-HD). The three independent seismic protection mechanisms of the design approach are illustrated in Fig. 1: The PVC 'sand-wich' seismic isolation, the steel wire mesh and the steel ties.

2.1. PVC 'sand-wich' seismic isolation

2.1.1. Mechanism and properties

The first seismic protection mechanism of the LC-HD design approach comprises an innovative seismic isolation system, defined as PVC 'sand-wich' seismic isolation. The PVC 'sand-wich' (PVC-s) seismic isolation is based on the inclusion of a thin layer of sand grains between two PVC surfaces. This configuration enables a sliding-rolling displacement of the upper PVC surface relative to the bottom PVC surface at a friction coefficient $\mu = 0.2$. This sliding-rolling motion between the two surfaces creates a seismic energy dissipation mechanism, which reduces substantially the acceleration response of the isolated structure for earthquake ground motion intensities higher than 0.2g. This novel seismic isolation system belongs to the family of Geotechnical Seismic Isolation (GSI) systems as defined by Tsang and Pitilakis [19].

2.1.2. Application

The proposed construction process for the application of this seismic isolation system to the prototype structure is the following: An excavation at a depth of 20 cm and horizontal dimensions 100 cm wider than the dimensions of the structure is performed first. This excavation facilitates the placement of a 15 cm thick hardcore layer allowing for the formation of a flat, rigid base below the sliding surface of the structure and a 5 cm thick sand layer. The hardcore layer that creates a rigid base below the seismic isolation system can comprise the construction of an unreinforced blinding layer. Therefore, the presented seismic isolation system leads to a substantial decrease of reinforced concrete volume compared to fixed-based conventional buildings, founded on large reinforced concrete footings. Furthermore, the presented seismic isolation system consists of only one reinforced concrete slab and an unreinforced blinding layer and facilitates a significant reduction of reinforced concrete volume compared to the existing highly engineered seismic isolation systems, requiring the construction of two reinforced concrete slabs above and below the seismic isolation system. This reinforced concrete volume reduction compared to the existing fixed-based and seismically isolated structures elucidates the resource efficiency of the presented novel seismic isolation system.

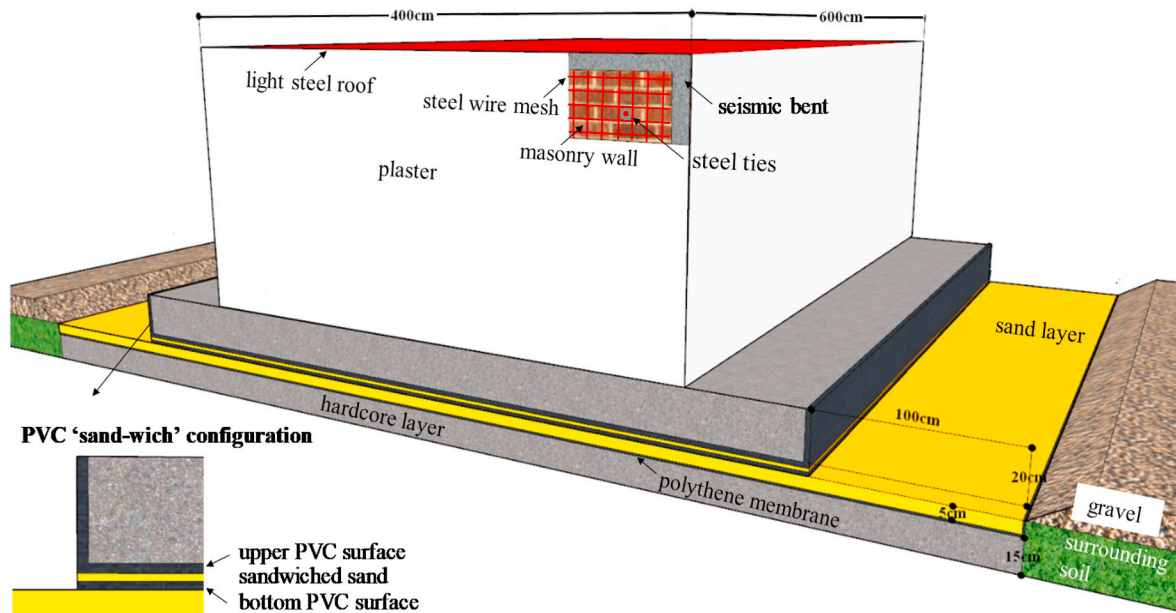A 20 cm thick and 30° inclined gravel layer is placed above the

Fig. 1. Application of the Low-Cost Hybrid-Design (LC-HD) approach to a prototype structure located in Nepal.

surrounding soil and around the sand layer to function as a stopper in the case of an unintended, excessive sliding motion of the structure. A polythene membrane is placed around the sand layer, thus preventing any material exchange between the layer and the surrounding soil. A PVC sheet is founded on the 5 cm thick sand layer to create the bottom surface of a 'sand-wich' configuration (Fig. 1). A thin layer of sand grains is uniformly distributed above the bottom PVC sheet using a 2 mm sieve, positioned at a height of 30 cm above the bottom PVC sheet. The upper PVC layer is then placed above the deposited sand grains, thus creating the upper surface of the 'sand-wich' configuration. A 20 cm thick concrete slab is casted on the upper 6 mm thick PVC surface, which remains as a permanent formwork above the sand layer. After the concrete slab hardens, the masonry structure can be constructed on the top of the slab.

2.2. Steel wire mesh

2.2.1. Mechanism and properties

The steel wire mesh is widely available at a low price and commonly used in developing countries, such as Nepal [35]. Therefore, the use of this mesh for seismic retrofitting of structures can create an efficient, low-cost seismic protection mechanism, which can significantly increase the resistance of unreinforced masonry walls to an out-of-plane failure during a strong earthquake ground motion excitation [31–33].

2.2.2. Application

The recommended steel wire diameter for the application of the steel mesh is 2 mm, while the recommended grid is 50mmx50mm. The mesh is continuously attached to both sides of each wall of the structure, bent on the top of the walls and bolted on the outer side of the concrete slab of the structure. The fixation of the mesh on the inner side of the walls is performed through its placement below an additional course of bricks, positioned above the concrete slab. The masonry walls are plastered after the attachment of the steel wire mesh.

2.3. Steel ties

2.3.1. Mechanism and properties

The steel ties comprise steel rebars that connect the opposite walls of the structure, thus providing an additional lateral restraint against the out-of-plane failure of masonry walls during an earthquake ground motion excitation. They are locally available at a low cost in developing

countries.

2.3.2. Application

Steel tie-bars threaded at their ends, are installed through holes and fixed on the facades of two opposite masonry walls of the prototype structure after the attachment of the steel mesh. The diameter of the steel ties that is recommended in this study is 6 mm.

2.4. Alternative configurations

2.4.1. Light roof

The construction of masonry structures with a light roof was extensive in Nepal after the 2015 Gorkha earthquake due to the ease of its application for Temporary Learning Centers (TLCs) enabling the continuation of the school function after the earthquake. A more permanent use of the existing light roof system is proposed in this study as a means of seismic mass and seismic demand reduction towards the protection of masonry structures from seismic damage.

2.4.2. High-strength mortar

The use of mortar with high-strength for the joints of the masonry walls of the structure is highly recommended in this study. The production of high-strength mortar can be implemented through the use of ordinary Portland cement, which is available in Nepal, with a cement to sand ratio of 1:4.

2.4.3. Strong corners

A well-constructed connection characterized by high interlocking between the bricks at the corners of the walls of masonry structures is recommended in this desigh approach. This construction technique is beneficial for the increase of the capacity of the walls against out-of-plane failure due to the activation of the shear resistance of the lateral walls before the occurrence of out-of-plane failure.

3. Experimental setup

3.1. Description of the components of the investigated structural system

A three times scaled-down 2.3t masonry model of the prototype structure is designed and constructed to facilitate the large-scale experimental investigation of the Low-Cost Hybrid-Design approach.

This experimental investigation is performed on the 3 m × 3 m, six-degree-of-freedom shaking table of University of Bristol. The experimental setup is presented in Fig. 2.

The length scale factor between the model and the prototype is 1/3. The brick size and mortar joint thickness are maintained between the model and the prototype structure: The 10cm × 6cm × 21.5 cm dimensions of the clay bricks and the 1 cm thick cement mortar joints used for the construction of the masonry model are selected to represent the brick dimensions and the mortar joint thickness that are commonly used for the construction of masonry structures in Nepal. However, the design of the model structure goes a step further and proposes the use of high-strength cement mortar, which is widely available in Nepal. The use of cement mortar with a cement to sand ratio value of 1:4 for the construction of the model masonry structure has led to a compression strength value of 6.6 MPa. This value, obtained through a compression test of mortar prisms at University of Bristol is significantly higher than the documented values of compression strength of 1.58 MPa for mud-mortar joints, obtained from experimental testing of mortar samples corresponding to low-strength Nepalese masonry structures [36]. Phaiju and Pradhan [37] determined experimentally in Nepal the compression strength value for a cement mortar of the same cement to sand ratio with the one used in this study (1:4) as 3.8 MPa. The cement-based high--strength mortar chosen in this experimental investigation can be applied on the site of the structure with appropriate guidance. However, the proposed LC-HD approach does not require the implementation of a specific model construction, but a mechanism of sliding beyond a specific earthquake ground motion intensity that is not dependent on the strength of the structure. Within this frame, the high strength of the structure investigated in this study is selected to demonstrate the high performance of a well-built structure, but most importantly to elucidate the beneficial role of the PVC 'sand-wich' seismic isolation.

The constructed masonry test structure characterized by the above described mechanical and geometrical properties was based on a 20 cm thick reinforced concrete base slab. The latter was resting on the PVC 'sand-wich' configuration, consisting of one upper 2 m × 1.3 m, 6 mm thick PVC sheet, an enclosed thin sand film and two bottom 2 m × 1.3 m, 6 mm thick PVC sheets, positioned symmetrically along the centroid of the bottom slab. The properties of the sand used in this study are summarized in Table 1. The amount of sand encapsulated between the two PVC sheets corresponds to a sand surface density of 750 g/m² with
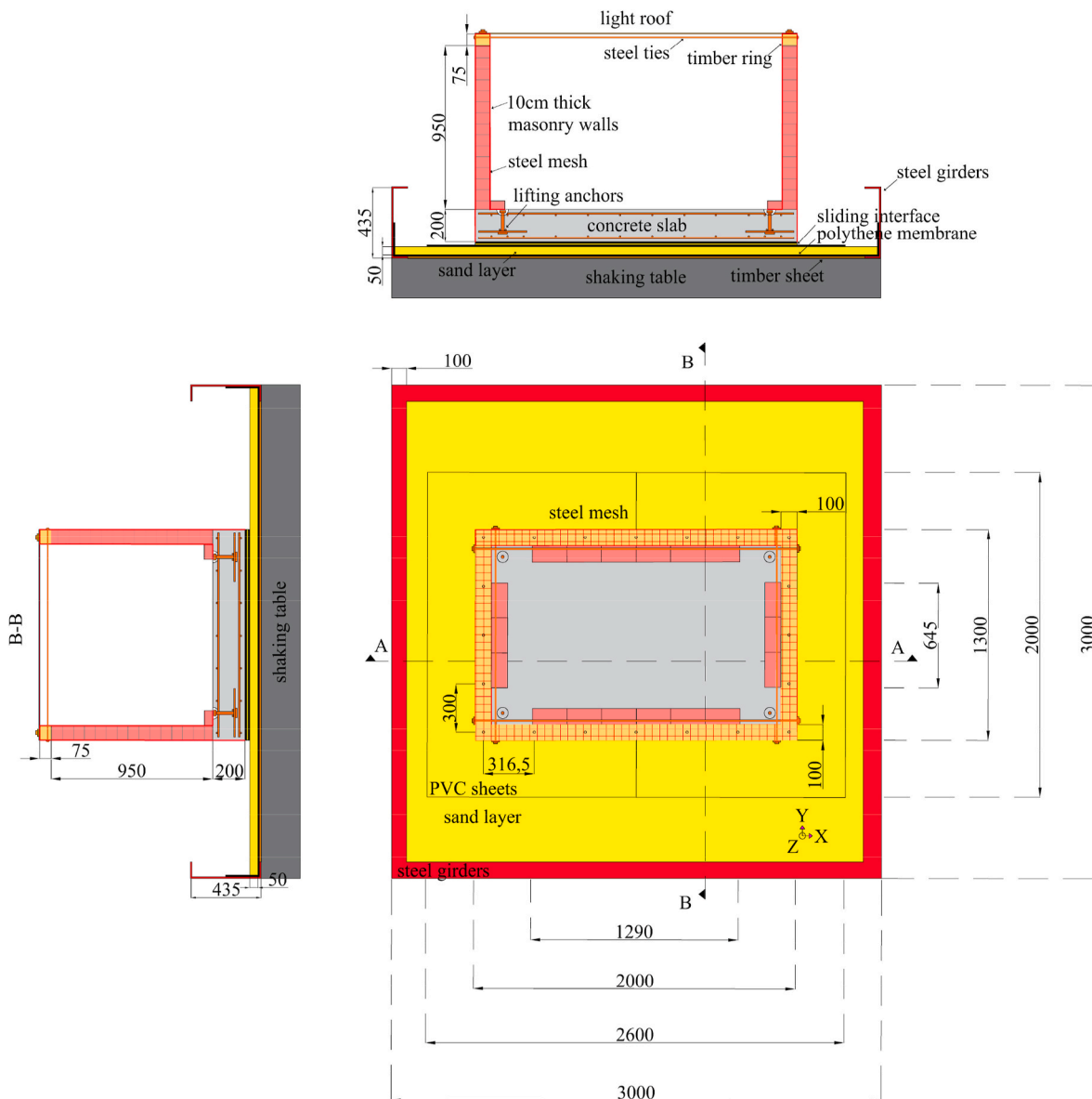

Fig. 2. Overview and cross-sections of the designed experimental setup (Dimensions in mm).

Table 1
Properties of the Leighton Buzzard 14–25 sand used in this study.

Specific gravity G_s	Void ratio e_{max}	Void ratio e_{min}	Mean size D_{50} [mm]	$C_u = D_{60}/D_{10}$	$C_g = D_{30}^2/D_{60}D_{10}$
2.65	0.84	0.53	0.883	1.439	0.996

respect to the projection area of the upper PVC surface on the bottom PVC surface. This sand surface density value was experimentally optimized [34] to yield a friction coefficient μ between the PVC sheets and the sandwiched sand equal to the design acceleration (in g) of the prototype structure in Nepal. The experimentally investigated seismically isolated structural system is founded on a 3 m × 3 m, 5 cm thick sand layer of the properties shown in Table 1 that was confined within a confinement box as shown in Fig. 2. The sand was deposited with zero-height drop, leading to a measured density of 1580 kg/m³. The sand layer is laterally enclosed by four C-shaped steel girders, which are fixed on the sides of the shaking table. A polythene membrane was placed between the girders and the sand layer (Fig. 2 [34]) to impede potential leakage of sand during the experimental investigation. The membrane was glued to timber sheets attached to the shaking table (Fig. 2 [34]) to prevent any unintentional sliding between the polythene surface and the shaking table.

The construction of the test-structure is illustrated in Fig. 3. The first step is building the walls using high-strength mortar and strong corners with high interlocking between the bricks (Fig. 3b). The second step is the attachment of the steel wire mesh. The 50mmx50mm steel wire mesh is attached to each of the walls of the constructed structure. Timber beams are bolted on the top course of the masonry walls to allow the placement of the roof of the structure. The steel mesh is bent above these timber beams on the top of the walls, thus enabling a continuous attachment on both sides of each wall and bolted on the surface of the concrete slab below each wall on both sides (Fig. 3d). After the fixation of the steel mesh on the four walls, the walls are plastered using a gypsum layer (Fig. 3e), thus following the current practice for masonry walls in Nepal and creating the maximum cohesion between the steel mesh and the masonry walls.

The third step of the application of the LC-HD approach is the

placement of four steel ties with a diameter of 6 mm through the constructed timber beams. The steel ties are fixed using bolts attached to the timber beams as shown in Fig. 3f. The placement of a simplified light timber roof on the top of the masonry walls is the last step of the application of the LC-HD approach before the positioning of the constructed structure, shown in Fig. 4. The use of a timber roof was chosen in these tests due to its easy transportability to and from the shaking table. However, the proposed design approach recommends the use of a light steel roof, which is already commonly used in Nepal.

3.2. Instrumentation

The acceleration and displacement response of the structure to the earthquake ground motion induced by the shaking table is measured through a dense grid of 27 uniaxial accelerometers and 100 displacement sensors, shown in Fig. 5. The three-dimensional motion of the displacement sensors (sensor size: 13.568 mm × 13.680 mm) is tracked by three infrared displacement cameras at a resolution of 0.1 mm. The synchronisation between the acceleration and displacement tracking systems enabled the accurate quantification of the response of the structure during the applied ground motion excitation.

3.3. Dimensional analysis

The dimensional analysis performed in this study facilitates the preservation of the similitude between the behavior of the experimentally investigated model and the prototype structure. Three dimensionless ratios Π_1, Π_2 and Π_3 were determined in this study as the fundamental parameters that govern this similitude: The ratio $\Pi_1 = \mu g/a_g$ (μ being the static friction coefficient, a_g is the peak ground acceleration of the ground motion excitation and g the acceleration of gravity) quantifies the acceleration required for the initiation of the rolling-sliding behavior of the interface (μg) with respect to a_g. Special emphasis is given in the design of the model structure on the maintenance of the same vertical stress for the foundation $\sigma'_v = 9$ kPa with respect to the prototype structure. The equivalent vertical stress conditions between the foundation stress on the model and the prototype structure facilitate the preservation of the frictional characteristics of the rolling-sliding interface, expressed through the friction coefficient μ

(a)   (b)   (c)

(d)   (e)   (f)
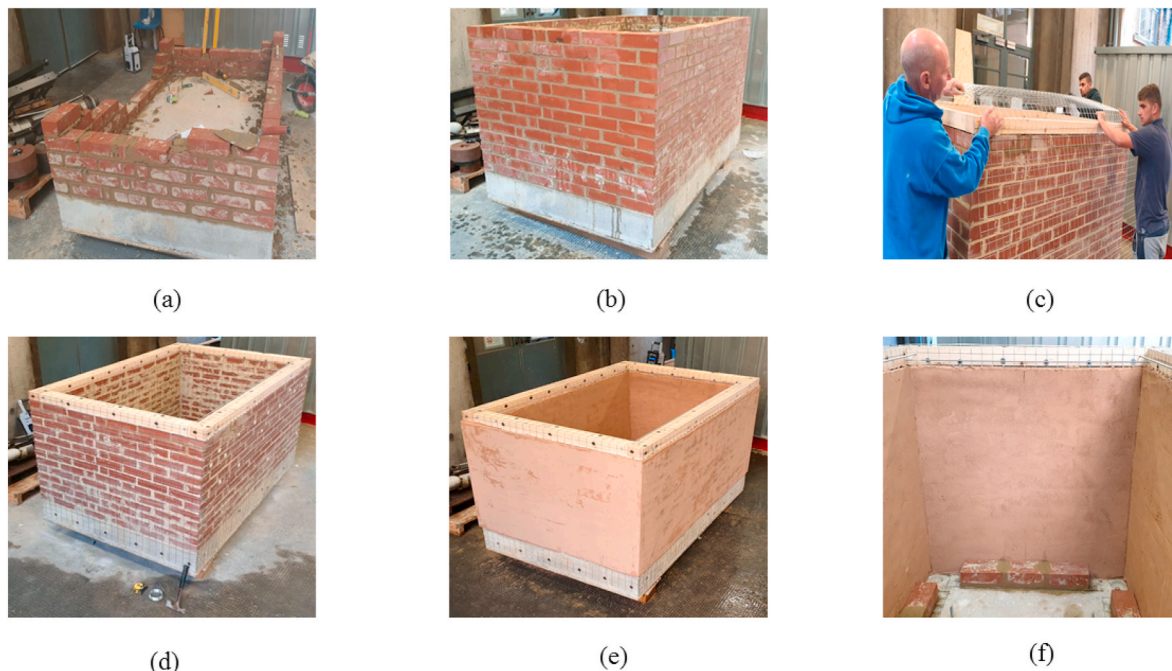
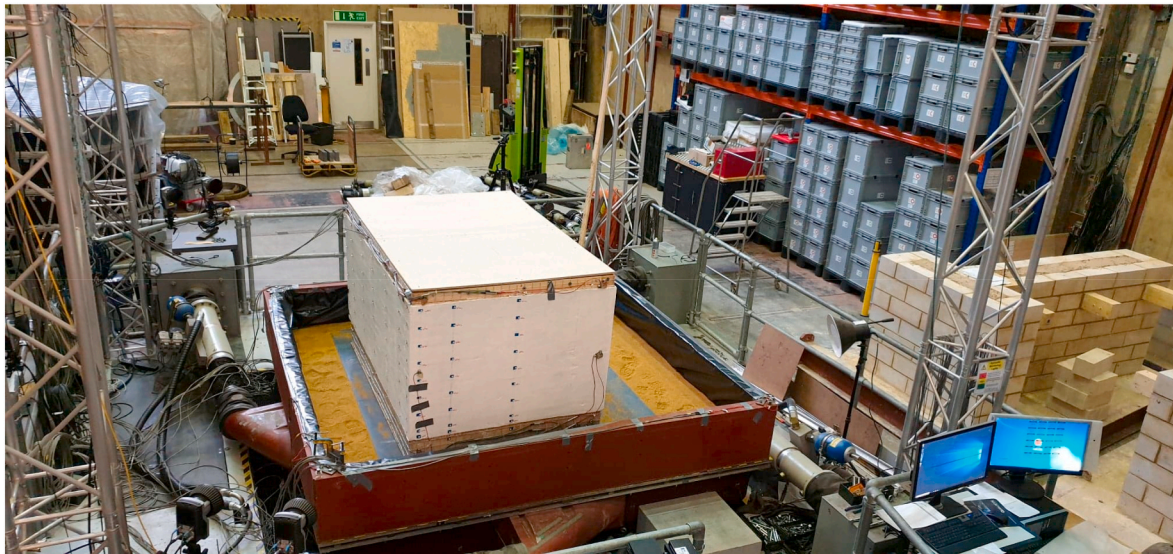**Fig. 3.** Application of the Low-Cost Hybrid-Design (LC-HD) approach to the model structure.

Fig. 4. Constructed experimental setup.

[28]. Hence, the ratio Π_1 is maintained between the two structures for ground motion excitations of the same a_g. The ratio $\Pi_2 = \tilde{T_y}/T_g$ represents the relation between the flexible-base period $\tilde{T_y}$ of the structure over the predominant period of the excitation T_g, defined as the period where the 5% velocity spectrum attains its maximum [38]. The model structure was designed to have a fixed-base vibration period $T_y = 0.1s$, equal with the corresponding value of the prototype structure. A white-noise test with amplitude $A = 0.05g$ and vibration frequency range $f = 0$–100Hz is performed for the determination of the flexible-base vibration period $\tilde{T_y}$ of the structural system. The experimentally estimated value was $\tilde{T_y} = T_y = 0.1s$, showing no occurrence of soil-structure interaction due to the low thickness of 5 cm of the sand layer below the bottom PVC surface, which is not adequate to elongate the vibration period of the structure. The desirable similarity between these periods and the design fixed-base period of the prototype structure leads to the preservation of the ratio Π_2 between the model and the prototype structure for ground motion excitations of the same frequency content. The ratio $\Pi_3 = t/h$ is the ratio of the thickness t of the masonry walls compared to their height h. This ratio has been determined as a fundamental parameter that influences significantly the out-of-plane behavior of masonry walls during earthquake ground motion excitation. The design of the 100 cm tall walls of the model structure with a thickness of 10 cm leads to a ratio $\Pi_3 = t/h = 10cm/100$ cm $= 0.1$. The corresponding value of this ratio for the prototype structure, designed with 30 cm thick, 300 cm tall masonry walls is $\Pi_3 = t/h = 30cm/300$ cm $= 0.1$, thus maintaining the similitude between the masonry model and the prototype structure. The aforementioned variables, dimensionless ratios and scale factors used in the dimensional analysis are summarized in Table 2.

3.4. Testing protocol

Four different earthquake ground motion intesities are used for the experimental investigation of the dynamic response of the structure presented in Fig. 2. The Chi-Chi 1999 recorded ground motion excitation, obtained from the PEER ground motion database [39] was scaled to four different peak ground acceleration levels a_g: 0.2g, 0.4g, 0.6g and 0.8g, as shown in Table 3. The selected ground motion record corresponds to a near-field motion with a pulse period $T_p = 1.3s$. The acceleration response spectrum for $a_g = 0.4g$ and the Fourier spectrum of the motion are shown in Fig. 6. The upper bound level of the scale factor has been selected to represent ground motion intensities that exceed the design hazard level in developing countries of high seismic hazard, such

as Nepal, which corresponds to an intensity $a_g = 0.4g$. A further increase of the ground motion intensity was not performed due to its expected low probability of occurrence. The model was excited in the Y-Direction of the experimental setup shown in Fig. 2.

4. Experimental investigation of the seismically isolated structure

The model structure was subjected to four different earthquake ground motion intensities shown in Table 3. The efficiency of the proposed PVC 'sand-wich' seismic isolation system as a core element of the proposed LC-HD approach is illustrated through the demonstration of the seismic response of the structure for three earthquake intensity levels.

The acceleration response on the top of the structure (mean value obtained by the accelerometers M1, M2 at the top of the structure shown in Fig. 5) subjected to the scaled Chi-Chi 1999 ground motion excitation with $a_g = 0.4g$ is shown in Fig. 7.

The desirable capping of the acceleration response due to the rolling-sliding response of the upper PVC layer against the bottom layer manifested itself at an acceleration level of 0.2g, as shown in the response of the structure during sliding (Fig. 7b). This seismic intensity level did not cause any damage to the structure designed using the proposed LC-HD approach as anticipated given the activated mechanism of sliding. The maximum sliding displacement of the structure (relative to the motion of the table) corresponding to this response was measured 9 cm, while the residual displacement was 6 cm (Fig. 8).

The initiation of sliding at an acceleration level of 0.2g was consistently observed during the excitation of the structure by the scaled Chi-Chi 1999 ground motion excitation with $a_g = 0.6g$ shown in Fig. 9. Interestingly, a different acceleration pulse has become critical for the sliding response of the structure subjected to this excitation, triggering a displacement of the structure on the opposite direction (Figs. 9b and 10b). As shown in Fig. 10, the maximum relative displacement attributed to this response is 16 cm and the corresponding residual value is 4 cm.

The response of the test structure due to its excitation by the strongest scaled Chi-Chi 1999 earthquake ground motion presented in this study with $a_g = 0.8g$ is shown in Fig. 11. The structure exhibits a repeatable rolling-sliding motion in both directions for successive pulses in this case (Fig. 11b), corresponding to the systematically observed acceleration cap of 0.2g in both directions ($+/-$ Y). This potentially disastrous ground motion has not triggered any observed damage to the
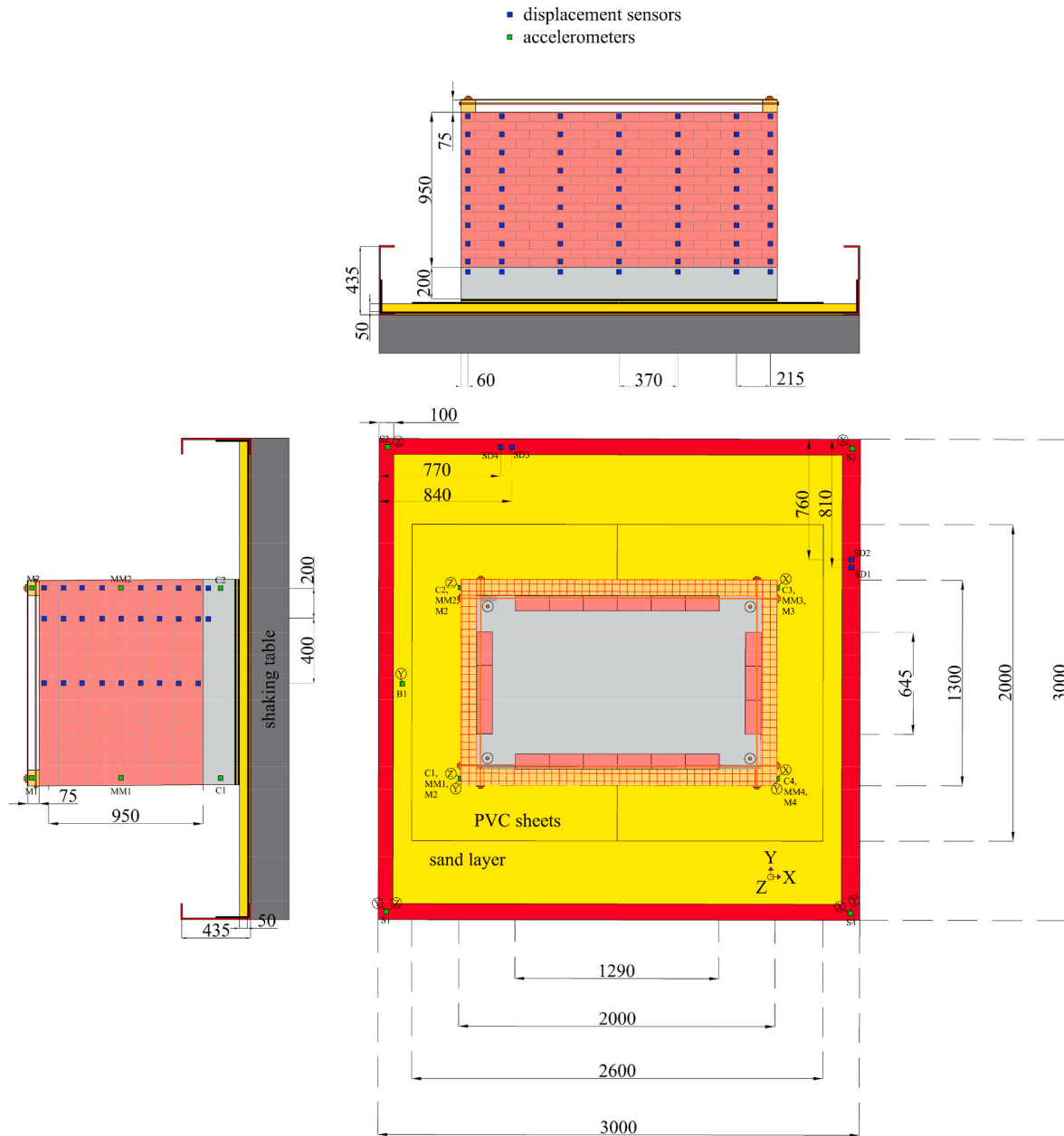
Fig. 5. Overview and side views of the instrumentation plan (Dimensions in mm).

Table 2
Variables and scale factors used in dimensional analysis.

Variables	Scale factors	Variables	Scale factors	Dimensionless ratios	Scale factors
Length L	1/3	Acceleration a	1	$\Pi_1 = \mu g / a_g$	1
Time t	1	Vertical stress σ'_v	1	$\Pi_2 = \tilde{T}_y / T_g$	1
Vibration period T $\tilde{y} = T_y$	1	Friction coefficient μ	1	$\Pi_3 = t/h$	1

Table 3
Testing protocol of recorded earthquake ground motion intensities used in this study (PEER NGA Database, 2018 [39]).

No.	Date	Earthquake and Site	M_w	R (km)	Component	Scaled a_g (g)
1	September 21, 1999	Chi-Chi, CHY080	7.6	2.69	CHY080-E	0.2
2	September 21, 1999	Chi-Chi, CHY080	7.6	2.69	CHY080-E	0.4
3	September 21, 1999	Chi-Chi, CHY080	7.6	2.69	CHY080-E	0.6
4	September 21, 1999	Chi-Chi, CHY080	7.6	2.69	CHY080-E	0.8

structure due to the activation of the PVC 'sand-wich' seismic isolation and the combined contribution of the seismic protection mechanisms, inherent in the LC-HD approach. As expected, this strong ground motion excitation led to the highest sliding displacement demand in the structure, reaching a maximum value of 24 cm and a residual value of 15 cm,

shown in Fig. 12. This significant sliding displacement demand of structures subjected to long-period ground motion excitation due to the pseudo-static action of the long-period seismic loading has been presented by Tsiavos et al. [40–42], Tsiavos and Stojadinovic [43] and
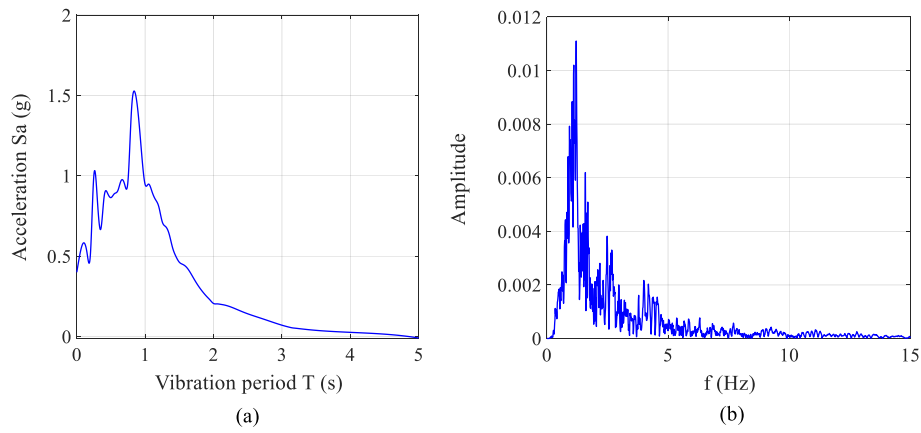
Fig. 6. (a) Acceleration response spectrum and (b) Fourier spectrum of the scaled Chi-Chi 1999 ground motion.
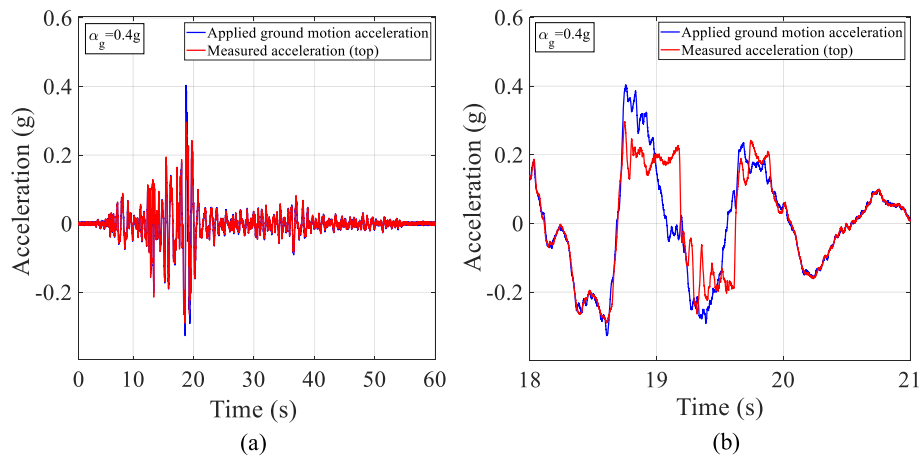

Fig. 7. (a) Full and (b) enlarged acceleration time history response at the top of the masonry structure (mean value obtained by the accelerometers M1, M2 at the top of the structure shown in Fig. 5) due to the applied Chi-Chi 1999 recorded ground motion excitation with $a_g = 0.4g$.
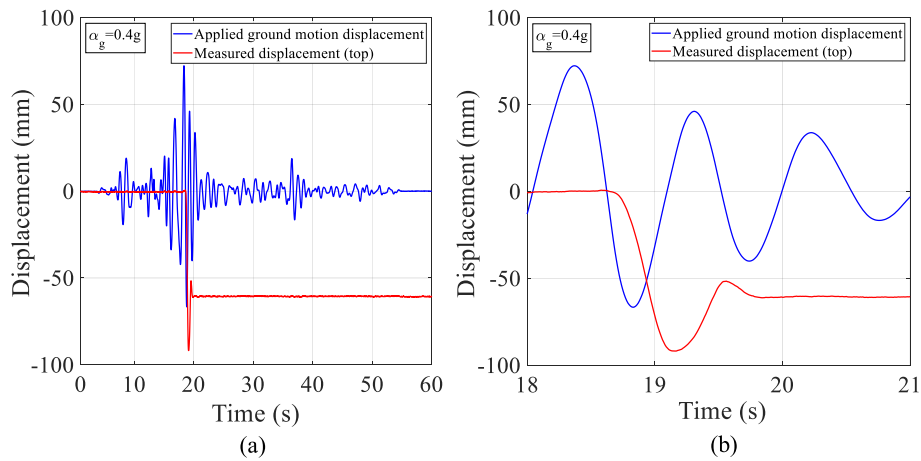

Fig. 8. (a) Full and (b) enlarged rolling-sliding displacement time history response of the structure (relative to the motion of the shaking table) due to the applied Chi-Chi 1999 recorded ground motion excitation with $a_g = 0.4g$.

Yaghmaei-Sabegh et al. [44].

5. Numerical investigation of the unretrofitted, fixed-based structure

The consistent, beneficial behavior of the proposed LC-HD approach towards the reduction of the seismic acceleration demand in the superstructure has been elucidated in the experimental investigation of the behavior of the seismically isolated masonry structure. However, the high strength of the experimentally investigated superstructure cannot lead to a direct assessment of the prevention of the potential seismic damage of a standard unreinforced masonry structure through the use of
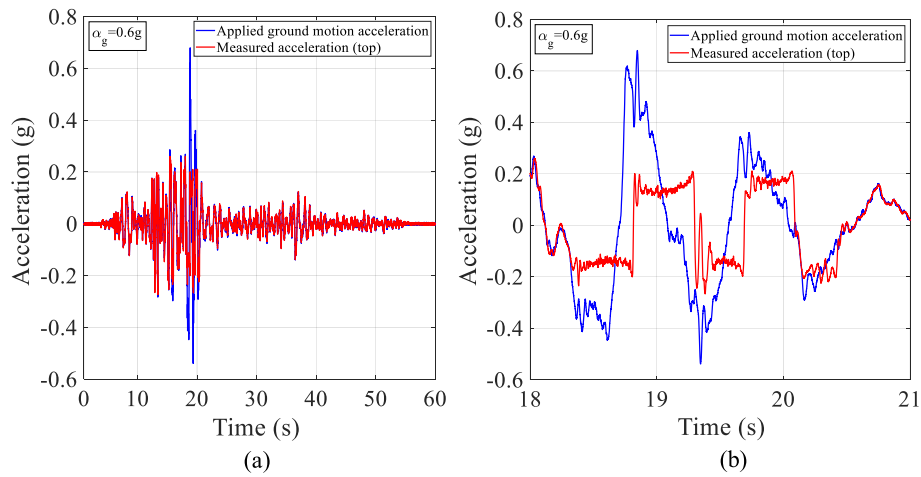
Fig. 9. (a) Full and (b) enlarged acceleration time history response on the top of the masonry structure (mean value obtained by the accelerometers M1, M2 at the top of the structure shown in Fig. 5) due to the applied Chi-Chi 1999 recorded ground motion excitation with $a_g = 0.6g$.
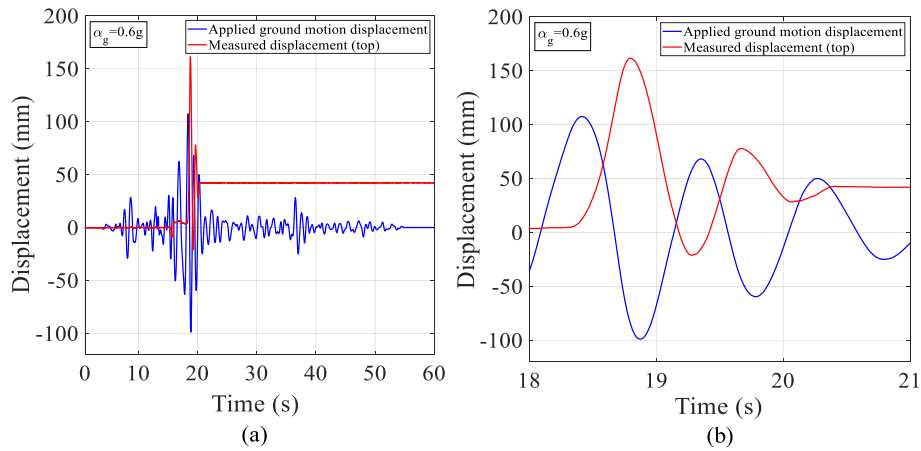

Fig. 10. (a) Full and (b) enlarged rolling-sliding displacement time history response of the structure (relative to the motion of the shaking table) due to the applied Chi-Chi 1999 recorded ground motion excitation with $a_g = 0.6g$.
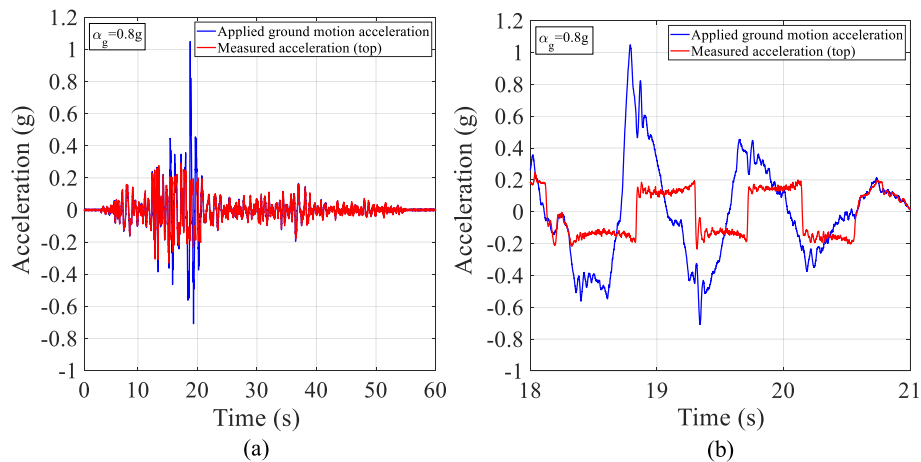

Fig. 11. (a) Full and (b) enlarged acceleration time history response on the top of the masonry structure (mean value obtained by the accelerometers M1, M2 at the top of the structure shown in Fig. 5) due to the applied Chi-Chi 1999 recorded ground motion excitation with $a_g = 0.8g$.

the presented design approach. Hence, a numerical model of the unreinforced, fixed-based masonry structure (URM) of the same dimensions with the experimentally tested structure (Fig. 13b) is developed in this study using the Finite Element Modelling (FEM) software Kratos

Multiphysics [45,46]. The application of the load to the fixed-based structure, shown in Fig. 13b, includes an incrementally increasing static horizontal load acting at 2/3 of the height of the wall through a stiff plate, representing the acting point of an equivalent seismic force.
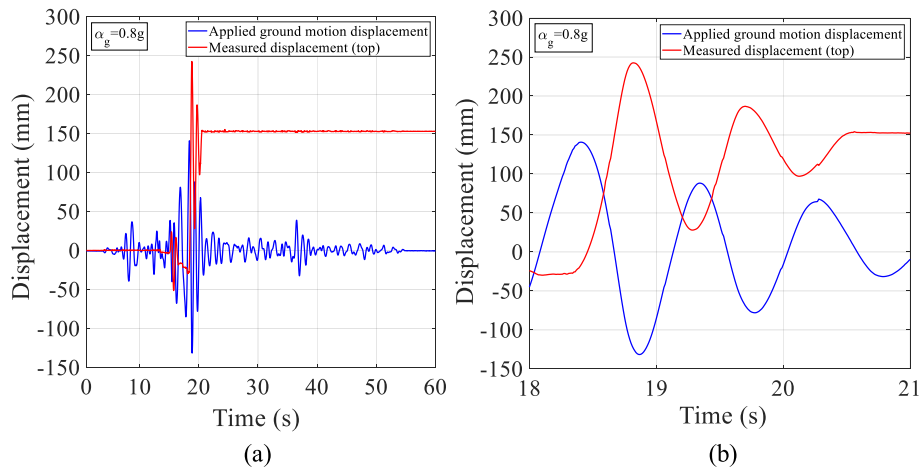
Fig. 12. (a) Full and (b) enlarged rolling-sliding displacement time history response of the structure (relative to the motion of the shaking table) due to the applied Chi-Chi 1999 recorded ground motion excitation with $a_g = 0.8g$.
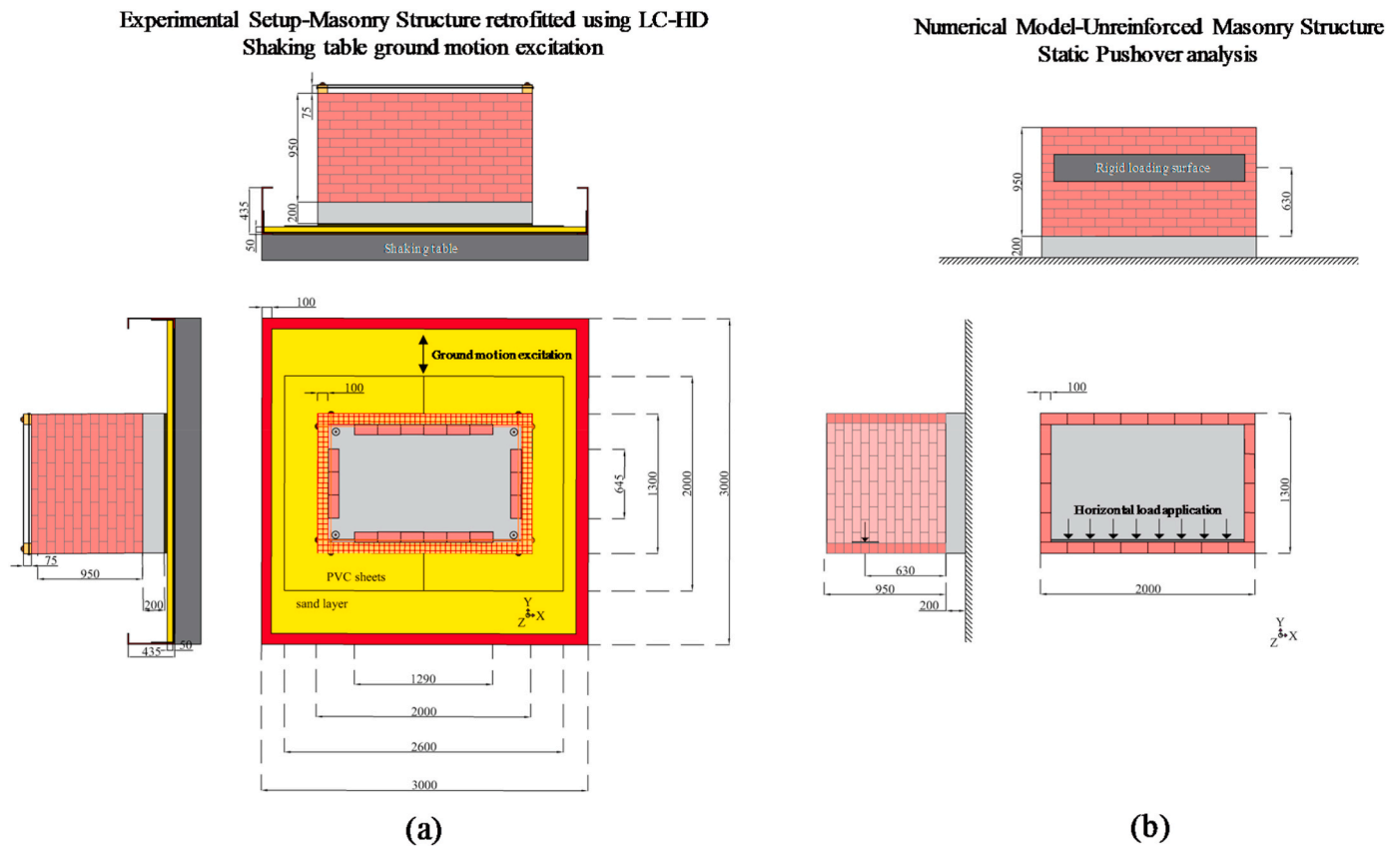

Fig. 13. (a) Layout of the experimental setup of the retrofitted masonry structure and (b) numerical model of the unretrofitted, fixed-based masonry structure (Dimensions in mm).

This numerical extrapolation is performed to show if the sliding mechanism alone would have prevented damage of an actual URM structure or a combination of the sliding mechanism with the retrofitting measures proposed in LC-HD approach is required for the protection of the URM structure from seismic damage.

The numerical model of the fixed-based structure, shown in Figs. 13b and 14a, is based on the FE discretization of bricks with continuum nonlinear elements and mortar with interface nonlinear elements (Fig. 14b [45]). The FE mesh size used for this numerical model was 3 cm. The model is founded on the multisurface plasticity approach, defining three failure surfaces for shear, tension and compression

(Fig. 14c [45]). The tensile and compression stress-strain material laws that govern the inelastic behavior of the discretized elements are presented in Fig. 14d and e, respectively [45]. The hardening and softening ranges of the compressive behavior are defined by three quadratic Bézier curves, whose form and shape are determined by the control stress-strain points (σ-ε), presented in Fig. 14e.

5.1. Calibration of masonry model

The numerical model simulates the seismic response of an unreinforced prototype masonry structure that is constructed with the
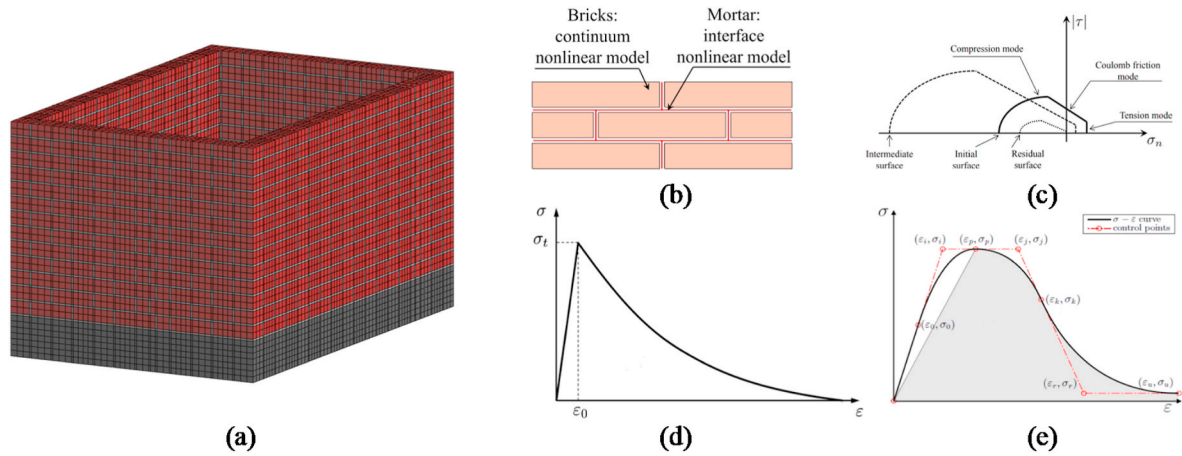
Fig. 14. (a) FE numerical model of the structure, (b) Discretization scheme (reprinted from Ref. [45]), (c) Tensile stress-strain behavior (reprinted from Ref. [45]) and (d) Compressive stress-strain behavior (reprinted from Ref. [45]).

following means and strength: mud-mortar, low construction quality and no attachment of steel ties, thus representing a weak interconnection between the walls as presented by Al Shawa et al. [47]. This low-strength mortar has been used in Nepal for the construction of the majority of the existing masonry structures in the past decades and is considered as a major source of the observed damage of these structures during the 2015 Gorkha earthquake [1,48]. The compression strength of mud mortar has been investigated through the conduction of numerous compression tests in Nepal. Indicative results from these compression tests conducted by Maskey et al. [36] are shown in Table 4. However, there is still a lack of experimental results and large amount of uncertainty on the value of the mortar tensile strength and the corresponding fracture energy, which are significant for the quantification of the out-of-plane behavior of masonry walls. A numerical model is always affected by model and aleatory uncertainties that influence the structural performance of structures [49,50]. Therefore, the numerical model presented in this study was calibrated based on the results obtained during the shear compression tests of 70cmx35cm, 70 cm tall wallets performed by Maskey et al. [36] in Nepal. The experimental setup applied in these tests and the design plans are shown in Fig. 15a, Fig. 15b, while the numerical model of the wallet using Kratos is illustrated in Fig. 15c.

The numerically simulated deformed shape of the wallet for a top horizontal displacement of 1.5 mm and the experimentally derived pushover force-displacement curve obtained during the static Pushover excitation of the wallet [36] for an applied vertical load of 1ton (vertical stress = 0.04 MPa) are presented in Figs. 15d and 16, respectively. The material parameters shown on Table 4 have been calibrated to match the experimentally derived pushover force-displacement curve. As shown in Fig. 16, the experimentally derived results are in very good agreement with the numerically reproduced static pushover response of the structure. Therefore, the material parameters presented on Table 4 have been chosen for the simulation of the static response of the presented numerical model of the unretrofitted masonry structure (Figs. 13b and 14a) to an incrementally applied static horizontal force.

5.2. Static pushover analysis of the model structure

The conduction of the static pushover analysis of the calibrated numerical model aims to elucidate what would be the seismic response of a fixed-based, unreinforced masonry structure (Fig. 13b) subjected to different levels of seismic hazard without the implementation of the proposed LC-HD approach. In this context, the numerical determination of the earthquake intensity that would trigger an out-of-plane failure of masonry walls as one of the most common failure mechanisms observed in 2015 Gorkha earthquake (Fig. 17) is of utmost importance.

A Newton-Raphson iteration scheme with a residual-based convergence criterion is used for the analysis. The numerically derived pushover force-displacement response of the unretrofitted fixed-based structure (Figs. 13b and 14a) and its bilinear idealization based on the principle of equal energy are demonstrated in Fig. 18. Three different damage states DS1, DS2 and DS3 have been identified to reflect the evolution of seismic damage in the structure for different top horizontal displacement levels: DS1 is quantified by the exceedance of 70% of the yield displacement ($0.7\delta_y = 0.001$ m) in the bilinear curve and manifests itself by the local exceedance of the tensile strength of the mud mortar between the walls, indicating initiation of cracking at the interface of the walls and deviation from the elastic stiffness of the model structure. DS2 is quantified by the displacement $\delta = 0.0038$ m corresponding to the maximum strength of the masonry structure characterizing the debonding of the facade wall from the transverse walls and the out-of-plane strength of the wall. DS3 is determined by the ultimate displacement capacity of the structure ($\delta_u = 0.0158$ m) and manifests itself by the collapse of the facade wall after its complete separation from the transverse walls.

The transformation of the presented pushover force-displacement curves to a capacity S_a-S_d acceleration-displacement spectrum of an equivalent SDOF system (ESDOF) facilitates the evaluation of the seismic performance of the structure for different earthquake intensity levels. The aforementioned transformation has been performed using the modification factors presented by Giordano et al. [48] and Doherty et al. [51]. The proposed formulation shown in Eq. (1) and (2) is based on the discretization of the wall in a predetermined number of elements n with mass m_i and displacement δ_i.

Table 4
Material parameters of the numerical model.

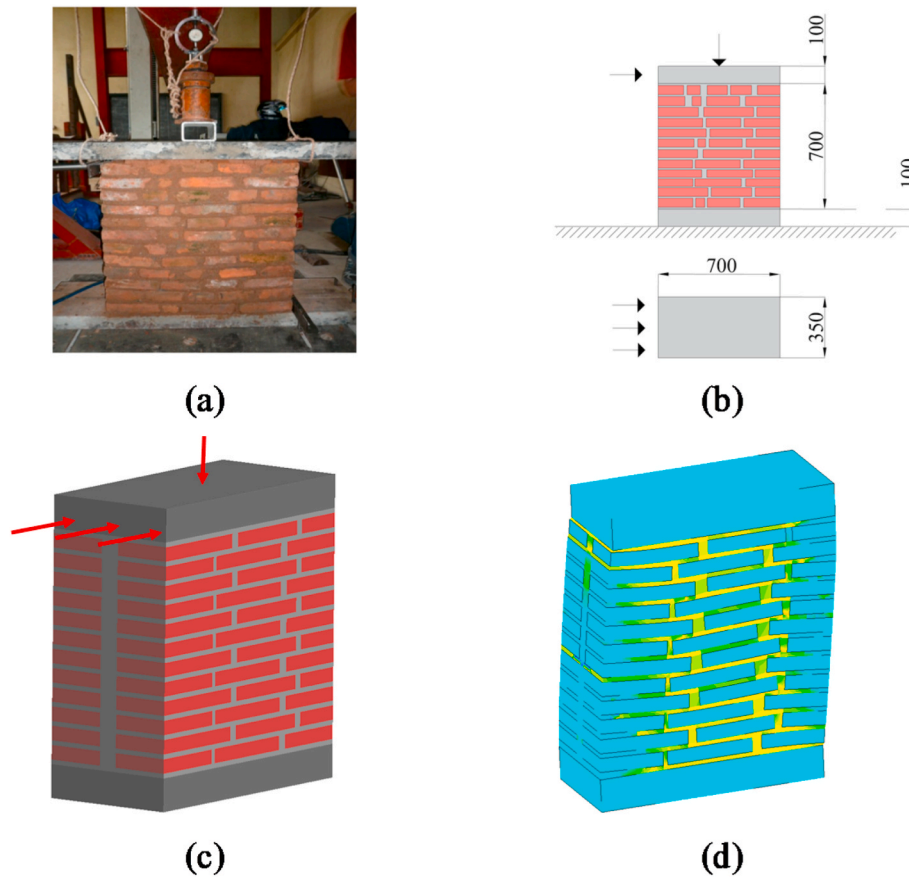|	Compression strength f'_c (MPa)	Tensile strength f'_t (MPa)	Elasticity modulus E (MPa)	Poisson ratio v	Fracture Energy-compression (N/mm)	Fracture Energy-tension (N/mm)	Density (kg/m³)
brick	11.03	2	3874	0.11	80	0.016	1768
mortar	1.58	0.02	794	0.25	6	0.08	1705

Fig. 15. (a) Experimental setup in Nepal reprinted from Ref. [36], (b) Design plans of the setup (Dimensions in mm), (c) Numerical simulation of the setup using Kratos Multiphysics and (d) Deformed shape of the wallet due to the applied loading for a top horizontal displacement of 1.5 mm.
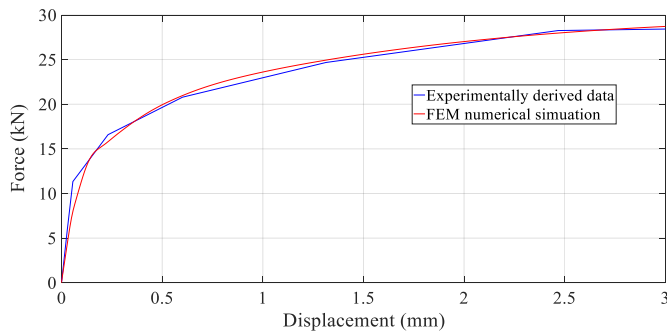

Fig. 16. Calibration of the numerical model based on experimental data.

$$S_a = \frac{F}{m_e}; \qquad m_e = \frac{\left(\sum\limits_{i=1}^{n} m_i \delta_i\right)^2}{\sum\limits_{i=1}^{n} m_i \delta_i^2} \tag{1}$$

$$S_d = \Delta_e; \qquad \Delta_e = \frac{\sum\limits_{i=1}^{n} m_i \delta_i^2}{\sum\limits_{i=1}^{n} m_i \delta_i} \tag{2}$$

where $m_e = (3/4)m$ for a wall with uniformly distributed mass and $\Delta_e = (2/3)\Delta$ for a parapet wall (Δ: top displacement of the wall) [48]

The Chi-Chi 1999 ground motion transformed to a S_a-S_d spectrum (Fig. 19) is chosen to represent the seismic acceleration demand during a hypothetical excitation of the fixed-based, unretrofitted model structure at two different intensity levels of the Chi-Chi 1999 ground motion excitation shown on Table 3: $a_g = 0.4g$ and $a_g = 0.6g$.

The N2 [52] performance-based seismic design and evaluation procedure is followed for the intersection of the idealized capacity pushover curve of the ESDOF system with the corresponding demand spectrum for the determination of the seismic performance of the structure at different intensity levels. The identification of this intersection, defining the performance point of the ESDOF structure for a seismic intensity of a PGA $a_g = 0.4g$ is shown in Fig. 20.

As presented in Fig. 20, the demand spectrum intersects the idealized capacity curve of the ESDOF system at a displacement $S_d = 0.84$ mm (Eq. (3)), reaching 90% of the yield displacement of the system. This displacement of the ESDOF system corresponds to a top displacement of 1.26 mm in the model structure (Eq. (2) and (4)), corresponding to the Damage State 1 (DS1) according to Fig. 18. Therefore, the Chi-Chi 1999

Fig. 17. Out-of-plane failure of brick masonry structures subjected to 2015 Gorkha earthquake (Credits: Dr. Rama Mohan Pokhrel).
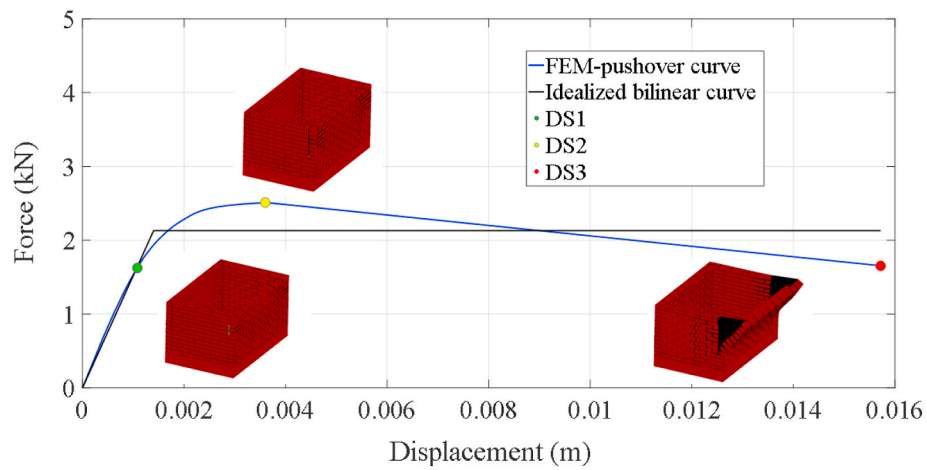

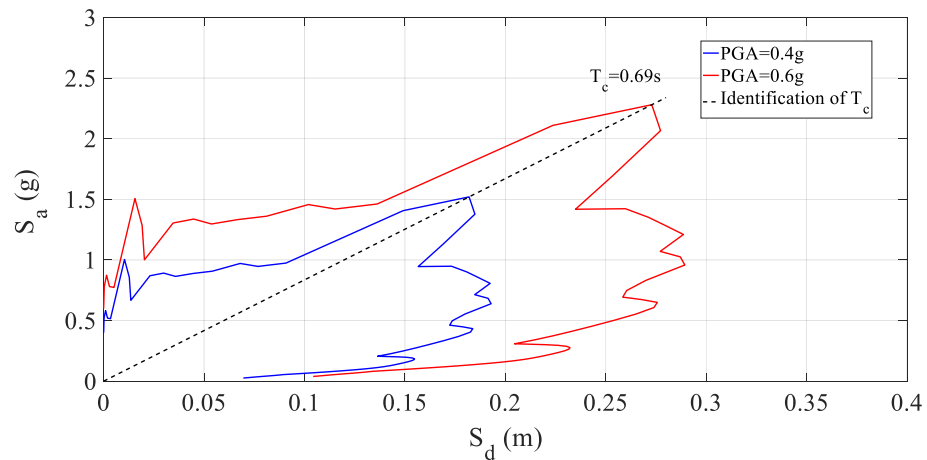**Fig. 18.** Numerically derived pushover curve, Damage States (DS) and idealized bilinear curve.

Fig. 19. Chi-Chi 1999 S_a-S_d spectrum for two different seismic intensity levels and identification of T_c.
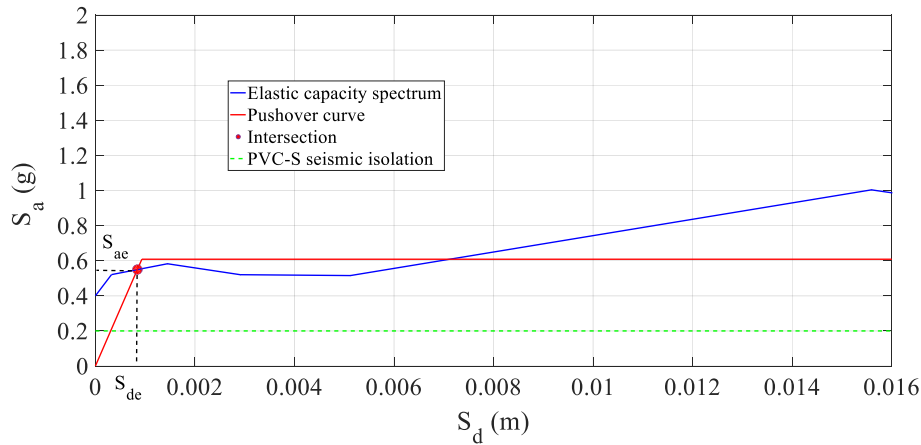
Fig. 20. Intersection of capacity-demand spectra using the N2 method for a PGA $a_g = 0.4g$.

ground motion excitation of the fixed-base, unreinforced model structure with a $a_g = 0.4g$ can lead to the initiation of cracking on the walls of the masonry structure (DS1).

$$S_{d(PGA=0.4g)} = 0.84\text{mm} \tag{3}$$

$$\Delta_{(PGA=0.4g)} = \left(\frac{3}{2}\right) S_{d(PGA=0.4g)} = 1.26\text{mm} \tag{4}$$

The efficiency of the proposed seismic isolation system presented in this study on the capping of the maximum acceleration response at a level of 0.2g is illustrated on Fig. 20, thus showing the beneficial effect of the system on the reduction of seismic damage compared to the response of the fixed-based, unretrofitted structure.

The seismic performance of the fixed-based, unretrofitted model structure, subjected to the Chi-Chi 1999 ground motion corresponding to $a_g = 0.6g$ is elucidated in Fig. 21.

As presented in the figure above, the strength of the ESDOF system is lower than the seismic demand in this case, thus inducing the inelastic response of the structure. This inelastic behavior, characterized by a reduction factor $R_\mu = 1.41$ leads to an ESDOF displacement of 3.76 mm (Eq. (5)), which corresponds to a top displacement of 4.22 mm on the model masonry structure. Evidently, this top displacement demand would lead to a severe damage of the structure for the $a_g = 0.6g$, as shown in Fig. 18. The capping of the maximum acceleration of the structure at 0.2g using the PVC-s seismic isolation, leading to a prevention of the damage of the structure compared to the fixed-base case, is shown on Fig. 21.

$$S_{d(PGA=0.6g)} = \frac{S_{de}}{R_\mu}\left(1 + (R_\mu - 1)\frac{T_c}{T^*}\right) = \frac{1.31\text{mm}}{1.41}\left(1 + (1.41 - 1)\frac{0.69\text{s}}{0.1\text{s}}\right) = 3.76\text{mm} \tag{5}$$

$$\Delta_{(PGA=0.6g)} = \left(\frac{3}{2}\right) S_{d(PGA=0.6g)} = 4.22\text{mm} \tag{6}$$

6. Conclusions

This study presents the design, the application and the large-scale experimental investigation of a low-cost hybrid design approach (LC-HD) for seismic damage mitigation in developing countries. The design of an innovative seismic isolation strategy, defined as PVC-'sand-wich' (PVC-s) seismic isolation lies in the core of the proposed LC-HD approach. This seismic isolation strategy is based on the inclusion ('sand-wiching') of a predetermined amount of sand grains between two PVC surfaces. This inclusion triggers a consistently observed rolling-sliding behavior of the structure founded on this PVC-s configuration, when subjected to earthquake ground motion excitation of intensity greater than 0.2g. However, the design approach proposed in this study is of a hybrid nature: The engineering of additional low-cost retrofitting measures aims at protecting the structure for earthquake intensities lower than the aforementioned sliding acceleration threshold of 0.2g. These measures include the attachment of a steel mesh and steel ties on masonry structures and additionally recommended good construction practices such as the placement of a light roof, the use of high-strength
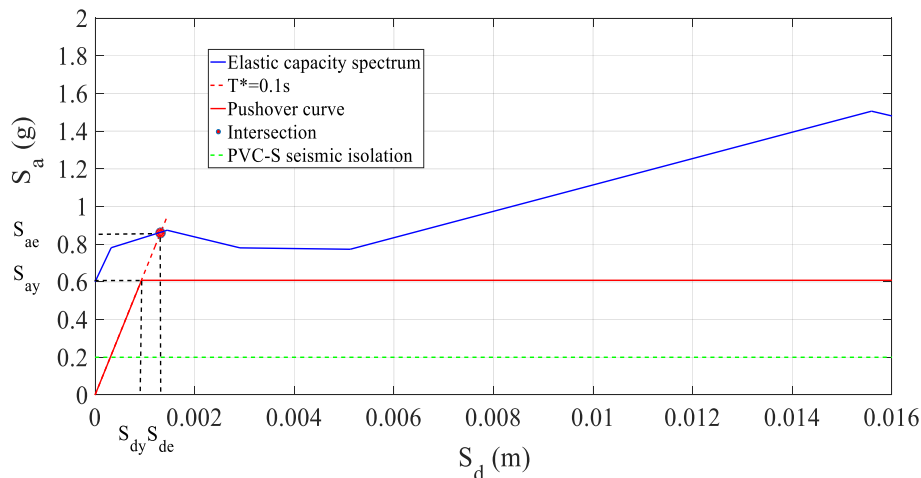

Fig. 21. Intersection of capacity-demand spectra using the N2 method for a PGA $a_g = 0.6g$.

mortar and the design of well-interconnected corners between the masonry walls.

The efficiency of the presented hybrid design approach consisting of the combination of the PVC-s seismic isolation and the aforementioned retrofitting measures has been experimentally tested in this study. A three-times scaled down model of a masonry structure, designed using the LC-HD approach has been subjected to four different amplitudes of earthquake ground motion excitation. The initiation of significant rolling-sliding behavior at a desirably low friction coefficient of 0.2 was observed for ground motion intensity levels exceeding the amplitude threshold of 0.2g. The combined effect of the capping of the maximum acceleration response of the structure through the proposed seismic isolation and the additional retrofitting measures has led to no manifestation of seismic damage and complete seismic protection of the structure even for ground motion excitations, exceeding the intensity level of 0.8g.

The illustration of the seismic damage on the corresponding unretrofitted, fixed-based masonry structure subjected to the same earthquake intensity levels with the undamaged isolated structure has been performed through a FEM numerical investigation. The numerical model simulates the seismic response of an unretrofitted structure constructed with low-strength mortar joints and weak interconnection between the walls at the corners. A static horizontal load has been incrementally applied on the structure to determine its pushover force-displacement response. Three different damage states have been defined to illustrate the seismic performance of the structure at different top displacement levels. The results of this simulation indicate initiation of cracking on the unretrofitted model structure at a seismic intensity $a_g = 0.4g$ and severe damage of the structure at a seismic intensity $a_g = 0.6g$.

The comparison of the response of the unretrofitted, fixed-base structure with the response of the same seismically isolated structure designed with the LC-HD approach yields initial evidence on the benefits of this design approach towards the low-cost protection of structures from seismic damage. The activation of the PVC-s seismic isolation at $a_g = 0.2g$ has been observed through the experimental investigation presented in this study, indicating a potential seismic protection of structures from damage at ground motion excitations above this intensity level. Within this context, the numerically illustrated damage of the unretrofitted, fixed-based structure, initiated at $a_g = 0.4g$ is experimentally not observed due to the activation of the PVC-s seismic isolation system. However, the proposed LC-HD approach entails the use of an ensemble of seismic protection mechanisms (steel wire, steel mesh) and utilization of good construction practices (high strength mortar, strong corners), which can protect the structure from seismic damage, even for the unintended scenario of no activation of the PVC-s seismic isolation system.

The experimental investigation of the seismic behavior of the presented masonry structure for varying intensities was conducted through the scaling of one earthquake ground motion record. Therefore, the influence of the variation of the ground motion frequency characteristics on the dynamic response of the masonry structure is not addressed in this study. Within this frame, the findings presented in this study can be generalized though the experimental investigation of the response of a seismically isolated masonry structure and the corresponding fixed-based structure to a wide range of earthquake ground motion records. Furthermore, the experimentally investigated masonry structure is an one-storey system with a limited number of degrees of freedom. Hence, the consideration of a structure of more degrees of freedom by future experimental studies would extend substantially the application range of the obtained results to more types of structures. The selection of the properties of the PVC and sand towards the optimization of the frictional and sliding behavior of the PVC-sand interface according to the type of the seismically isolated structure could also be addressed by future studies to provide a selection protocol that further improves the attractive frictional characteristics of the PVC-s seismic isolation. The earthquake ground motion excitation of an unreinforced masonry

structure of low strength subjected to a wide ground motion ensemble is scheduled to be performed using the shaking table of University of Bristol, thus further increasing the impact of the proposed LC-HD design approach.

Declaration of competing interest

The authors declare that they have no known competing financial interests or personal relationships that could have appeared to influence the work reported in this paper.

Acknowledgements

References

[1] Brando G, Rapone D, Spacone E, O'Banion MS, Olsen MJ, Barbosa AR, Faggella M, Gigliotti R, Liberatore D, Russo S, Sorrentino L, Bose S, Stavridis A. Damage reconnaissance of unreinforced masonry bearing wall buildings after the 2015 Gorkha, Nepal, earthquake. Earthq Spectra 2017;33:243–73.

[2] Novelli V, Kloukinas P, De Risi R, Kafodya I, Ngoma I, Macdonald J, et al. Seismic mitigation framework for non-engineered masonry buildings in developing countries: application to Malawi in the east African rift. Book title: resilient structures and infrastructure. Publisher: Springer Singapore; 2019 [Chapter 8].

[3] Unesco. Diversity of cultural expressions: IFCD List of developing countries. Available in part at: https://en.unesco.org/creativity/files/ifcd-list-elegible-developing-countries-en.

[4] Constantinou MC, Tadjbakhsh IG. The optimum design of a base isolation system with frictional elements. Earthq Eng Struct Dynam 1984;12:203–14.

[5] Buckle IG, Nagarajaiah S, Ferrell K. Stability of elastomeric isolation bearings: experimental study. J Struct Eng 2002;128(1):3–11.

[6] Kelly JM. Aseismic base isolation: review and bibliography. Soil Dynam Earthq Eng 1986;5(3):202–16.

[7] Takewaki I. Robustness of base-isolated high-rise buildings under code specified ground motions. Struct Des Tall Special Build 2008;17(2):257–71.

[8] De Luca A, Guidi LG. State of art in the worldwide evolution of base isolation design. Soil Dynam Earthq Eng 2019;125:105722.

[9] Whittaker AS, Sollogoub P, Kim MK. Seismic isolation of nuclear power plants: past, present and future. Nucl Eng Des 2018;338:290–9.

[10] Castaldo P, Tubaldi E. Influence of ground motion characteristics on the optimal single concave sliding bearing properties for base-isolated structures. Soil Dynam Earthq Eng 2018;104:346–64.

[11] Giarlelis C, Keen J, Lamprinou E, Martin V, Poulios G. The seismic isolated stavros niarchos foundation cultural center in athens (SNFCC). Soil Dynam Earthq Eng 2018;114:534–47.

[12] Mazza F, Mazza M, Vulcano A. Base-isolation systems for the seismic retrofitting of r.c. framed buildings with soft-storey subjected to near-fault earthquakes. Soil Dynam Earthq Eng 2018;109:209–21.

[13] Wagner PR, Dertimanis VK, Chatzi E, Beck JL. Robust-to-uncertainties optimal design of seismic metamaterials. J Eng Mech 2018;144(3):04017181.

[14] Gazetas G. 4th Ishihara lecture: soil–foundation–structure systems beyond conventional seismic failure thresholds. Soil Dynam Earthq Eng 2015;68:23–39.

[15] Anastasopoulos I, Kourkoulis R, Gelagoti F, Papadopoulos E. Response of SDOF systems on shallow improved sand: an experimental study. Soil Dynam Earthq Eng 2012;40:15–33.

[16] Karatzia X, Mylonakis G, Bouckovalas G. Seismic isolation of surface foundations exploiting the properties of natural liquefiable soil. Soil Dynam Earthq Eng 2019; 121:233–51.

[17] Banović I, Radnić J, Grgić N, Matešan D. The use of limestone sand for the seismic base isolation of structures. Adv. Civ. Eng. 2018;2018. Article ID 9734283.

[18] Tsang HH, Lam NTK, Yaghmaei-Sabegh S, Sheikh MN, Indraratna B. Geotechnical seismic isolation by scrap tire–soil mixtures. Proceedings of the 5th international conference on recent Advances in geotechnical earthquake engineering and soil dynamics. San Diego, California: U.S.; May 24–29, 2010.

[19] Tsang HH, Pitilakis K. Mechanism of geotechnical seismic isolation system: analytical modeling. Soil Dynam Earthq Eng 2019;122:171–84.

[20] Mitoulis SA, Palaiochorinou A, Georgiadis I, Argyroudis S. Extending the application of integral frame abutment bridges in earthquake-prone areas by using novel isolators of recycled materials. Earthq Eng Struct Dynam 2016;45(14): 2283–301.

[21] Tsiavos A, Alexander N, Diambra A, Ibraim E, Vardanega P, Gonzalez-Buelga A, et al. A sand-rubber deformable granular layer as a low-cost seismic isolation strategy in developing countries: experimental investigation. Soil Dynam Earthq Eng 2019;125:105731.

[22] Amontons, G.: De la resistance causee dans les machines. Mem. Acad. Roy. Sci. 1699; 206–226.

[23] Tabor D. The mechanism of rolling friction. II. The elastic range. Proc Roy Soc Lond Math Phys Sci 1955;229:198–220.

[24] Eldredge KR, Tabor D. The mechanism of rolling friction. I. The plastic range. Proc Roy Soc Lond Math Phys Sci 1955;229:181–98.

[25] O'Rourke TD, Druschel SJ, Netravali AN. Shear strength characteristics of sand-polymer interfaces. Journal of Geotechnical Engineering 1990;116(3):451–69. ASCE.

[26] Fang L, Kong XL, Su JY, Zhou QD. Movement patterns of abrasive particles in three-body abrasion. Wear 1993;162:782–9.

[27] Dietz MS. Developing an holistic understanding of interface friction using sand with direct shear apparatus. University of Bristol; 2000. PhD Thesis.

[28] Lings ML, Dietz MS. The peak strength of sand-steel interfaces and the role of dilation. Soils Found 2005;45(6):1–14.

[29] de Leeuw LW, Diambra A, Dietz MS, Mylonakis G, Milewski H. Cyclic polypropylene pipeline coating interface strength with granular materials at low stress. In: Proceedings of the XVII ECSMGE; 2019. Reykjavik.

[30] Furinghetti M, Pavese A, Quaglini V, Dubini P. Experimental investigation of the cyclic response of double curved surface sliders subjected to radial and bidirectional sliding motions. Soil Dynam Earthq Eng 2019;117:190–202.

[31] ElGawady M, Lestuzzi P, Badoux M. A review of conventional seismic retrofitting techniques for URM. In: 13th International brick and block masonry conference; 2004. Amsterdam.

[32] Shermi C, Dubey RN. Study on out-of-plane behaviour of unreinforced masonry strengthened with welded wire mesh and mortar. Construct Build Mater 2017;143: 104–20.

[33] Kouris LAS, Triantafillou TC. State-of-the-art on strengthening of masonry structures with textile reinforced mortar. Construct Build Mater 2018;188(10): 1221–33.

[34] Tsiavos A, Sextos A, Stavridis A, Dietz M, Dihoru L, Nicholas A, et al. Large-scale experimental investigation of a low-cost PVC 'sand-wich' (PVC-s) seismic isolation for developing countries. Earthquake Spectra 2020;36(4):1886–911.

[35] Shrestha H, Pradhan S, Guragain R. Experiences on retrofitting of low strength masonry buildings by different retrofitting techniques in Nepal. 2012. 15th World Conference on Earthquake Engineering, Lisbon, Portugal.

[36] Research center for disaster mitigation of urban cultural heritage. Disaster risk management for the Historic City of Patan, Nepal. Japan: Kyoto; 2012.

[37] Phaiju S, Pradhan PM. Experimental work for mechanical properties of brick and masonry panel. Journal of Science and Engineering Nepal 2018;5(8):51–7.

[38] Mylonakis G, Gazetas G. Seismic soil-structure interaction: beneficial or detrimental? J Earthq Eng 2000;4(3):277–301.

[39] PEER NGA Strong Motion Database. Pacific earthquake engineering research center, University of California, Berkeley. https://ngawest2.berkeley.edu/. Accessed 08 October 2018.

[40] Tsiavos A, Mackie KR, Vassiliou MF, Stojadinovic B. Dynamics of inelastic base-isolated structures subjected to recorded ground motions. Bull Earthq Eng 2017;15 (4):1807–30.

[41] Tsiavos A, Schlatter D, Markic T, Stojadinovic B. Experimental and analytical investigation of the inelastic behavior of structures isolated using friction pendulum bearings. Procedia engineering 2017;199:465–70.

[42] Tsiavos A, Haladij P, Sextos A, Alexander NA. Analytical investigation of the effect of a deformable sliding layer on the dynamic response of seismically isolated structures. Structures 2020;27:2426–36.

[43] Tsiavos A, Stojadinovic B. Constant yield displacement procedure for seismic evaluation of existing structures. Bull Earthq Eng 2018;17(4):2137–64.

[44] Yaghmaei-Sabegh S, Safari S, Ghayouri KA. Estimation of inelastic displacement ratio for base-isolated structures. Earthq Eng Struct Dynam 2017;47:634–59.

[45] Petracca M, Pela L, Rossi R, Zaghi S, Camata G, Spacone E. Micro-scale continuous and discrete numerical models for nonlinear analysis of masonry shear walls. Construct Build Mater 2017;149:296–314.

[46] Dadvand P, Rossi R, Oñate E. An object-oriented environment for developing finite element codes for multi-disciplinary applications. Arch Comput Methods Eng 2010; 17(3):253–97.

[47] Al Shawa O, de Felice G, Mauro A, Sorrentino L. Out-of-plane seismic behaviour of rocking masonry walls. Earthq Eng Struct Dynam 2012;41(5):949–68.

[48] Giordano N, De Luca F, Sextos A. Out-of-plane closed-form solution for the seismic assessment of unreinforced masonry schools in Nepal. Eng Struct 2019;203: 109548.

[49] Castaldo P, Gino D, Mancini G. Safety formats for non-linear finite element analysis of reinforced concrete structures: discussion, comparison and proposals. Eng Struct 2019;193:136–53.

[50] Castaldo P, Gino D, Bertagnoli G, Mancini G. Resistance model uncertainty in non-linear finite element analyses of cyclically loaded reinforced concrete systems. Eng Struct 2020;211:110496.

[51] Doherty K, Griffith MC, Lam N, Wilson J. Displacement-based seismic analysis for out-of-plane bending of unreinforced masonry walls. Earthq Eng Struct Dynam 2002;31:833–50.

[52] Fajfar P. Capacity spectrum method based on inelastic demand spectra. Earthq Eng Struct Dynam 1999;28:979–93.